# Wrist: Anatomy and MRI Optimization

6

Asako Yamamoto, Brady K. Huang, and Christine B. Chung

## Osseous Anatomy of the Wrist

The wrist joint includes the osseous structures of the distal radius and ulna, carpal bones, and metacarpal bases (Fig. 6.1). The carpal bones form the proximal (scaphoid, lunate, triquetrum) and distal (trapezium, trapezoid, capitate, hamate) carpal rows that are stabilized by intrinsic and extrinsic ligaments to act as a single intercalated segment. The radiocarpal articulation is formed by the distal surface of the radius with the triangular fibrocartilage serving as a soft tissue articular surface extension distal to the ulna. The articular surface of the radius has two shallow fossae that accommodate the scaphoid and lunate. At the dorsum of the distal radius, an osseous prominence is present that serves as an anatomic landmark for the extensor tendons. This is referred to as Lister's tubercle. The midcarpal joint lies between the proximal and distal carpal rows. The articular surfaces of the carpal bones are normally aligned into three arcs (Gilula's arcs) [1]. The proximal (arc I) and distal (arc II) articular surfaces of the proximal row and the opposing joint surface formed by the convexity of the distal row (arc III) comprise the three arcs. Those opposing articular surfaces should be parallel to one another with symmetrical joint spaces [2]. The pisiform is generally considered a sesamoid and not officially housed in either carpal row [3]. Interruption of a uniformly parallel configuration of the joint spaces or a step-off at the articular surface is secondary findings that suggest insufficiency of stabilizing ligamentous structures. When the "ring" of the intercalated segment is broken, the carpal alignment may be affected. Two common anatomical variants can mimic carpal arc step-offs: (1) triquetrum shorter in its proximal-distal dimension than the adjacent lunate (Fig. 6.2a) and (2) proximally prominent hamate articulating with lunate (type II lunate) (Fig. 6.2b). The former variation results in lunotriquetral step-off, whereas the latter affects the third carpal arc. The prevalence of the type 2 lunate was demonstrated to be 50–57% in radiologic studies and up to 73% in cadaveric studies [4–6]. The mean size of the facet was reported as 4.5 mm (range, 2–6 mm) in type II lunate on coronal view [5].

The normal longitudinal axes through the third metacarpal, capitate, lunate, and radius should superimpose, with 0 to 30° (the capitolunate angle) on lateral radiographs [6] (Fig. 6.3a, b). Also, the angle formed between the long axis of the lunate and the scaphoid ranges between 30 and 60° normally (the scapholunate angle). Those

A. Yamamoto · B. K. Huang
Department of Radiology, University of California San Diego, La Jolla, CA, USA

C. B. Chung (✉)
Department of Radiology, University of California San Diego, La Jolla, CA, USA

Department of Radiology, VA San Diego Healthcare System and University of California San Diego, La Jolla, CA, USA
e-mail: cbchung@health.ucsd.edu



B. U. Casagranda (ed.), *MRI of the Upper Extremity*, https://doi.org/10.1007/978-3-030-81612-4_6

parameters are essential for the evaluation of volar intercalated segmental instability (VISI) or dorsal intercalated segment instability (DISI) (Fig. 6.3c–f). Although recognition of a DISI or VISI configuration on MR images can be useful in the assessment of carpal bone alignment, correlation with radiographs is indispensable [7]. The axis of each bone is assessed in the following way: a line parallel to the center of the radial shaft, a line through the midpoints of the lunate proximal and distal articular surfaces, a line through the centers of the capitate head and its distal articular surface, and a line through the midpoints of the scaphoid proximal and distal poles.

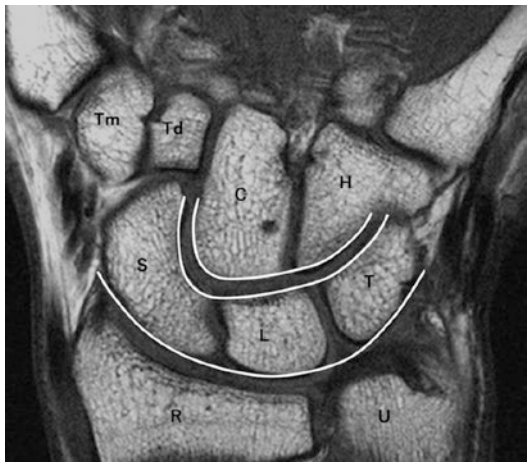


**Fig. 6.1** Coronal T1-weighted image of the wrist shows anatomy of carpal bones with lines of Gilula's arc. Abbreviations: Tm Trapezium, Td Trapezoid, C Capitate, H Hamate, S Scaphoid, L Lunate, T Triquetrum, R Radius, U Ulna

To evaluate the anatomical profile of the distal radius, there are three common ways of measurement based on radiographs: radial inclination, radial length, and volar tilt. Radial inclination is measured as the angle between a line drawn from the tip of the radial styloid to the ulnar head articular surface and a second line perpendicular to the longitudinal axis of the radius (Fig. 6.4a). It ranges from 13 to 30° (average 23 degrees) [8, 9]. Radial length can also be measured on PA radiographs or MRI on the coronal plane, normally ranging from 11 to 22 mm (average 12 mm) (Fig. 6.4a). The volar tilt of the radius is measured on the sagittal plane as the angle between a line drawn tangentially across the most distal

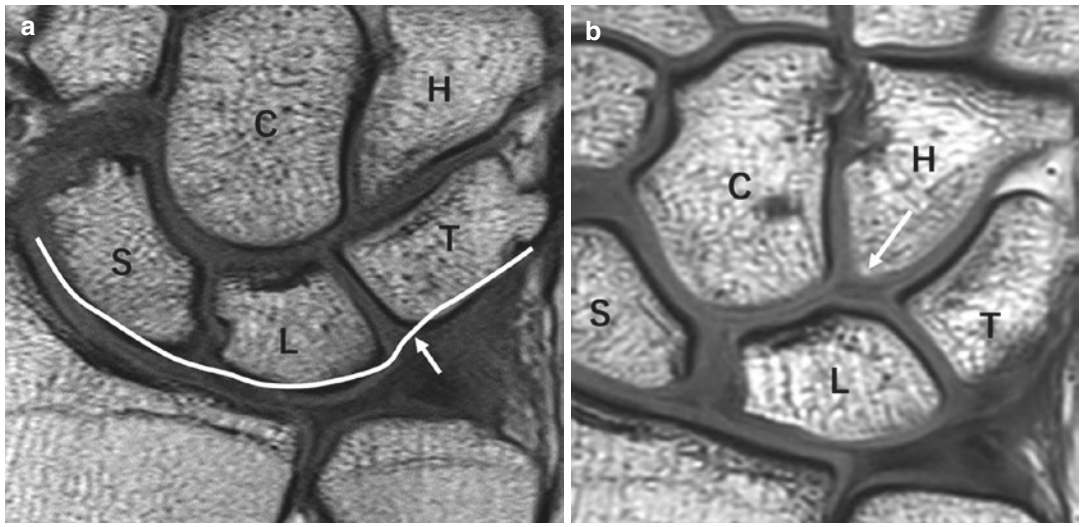


**Fig. 6.2** Two common normal variants that mimic carpal arch step-off: (**a**) Short triquetrum. Proximal-distal dimension of triquetrum is shorter than adjacent lunate (L), creating lunotriquetral step-off (arrow) of first carpal arc. Note the proximal configuration of the hamate (H), type I lunate (single distal articular facet for capitate). (**b**) Type II lunate. An additional distal articular facet medially for hamate, affecting the third carpal arc continuity (arrow)

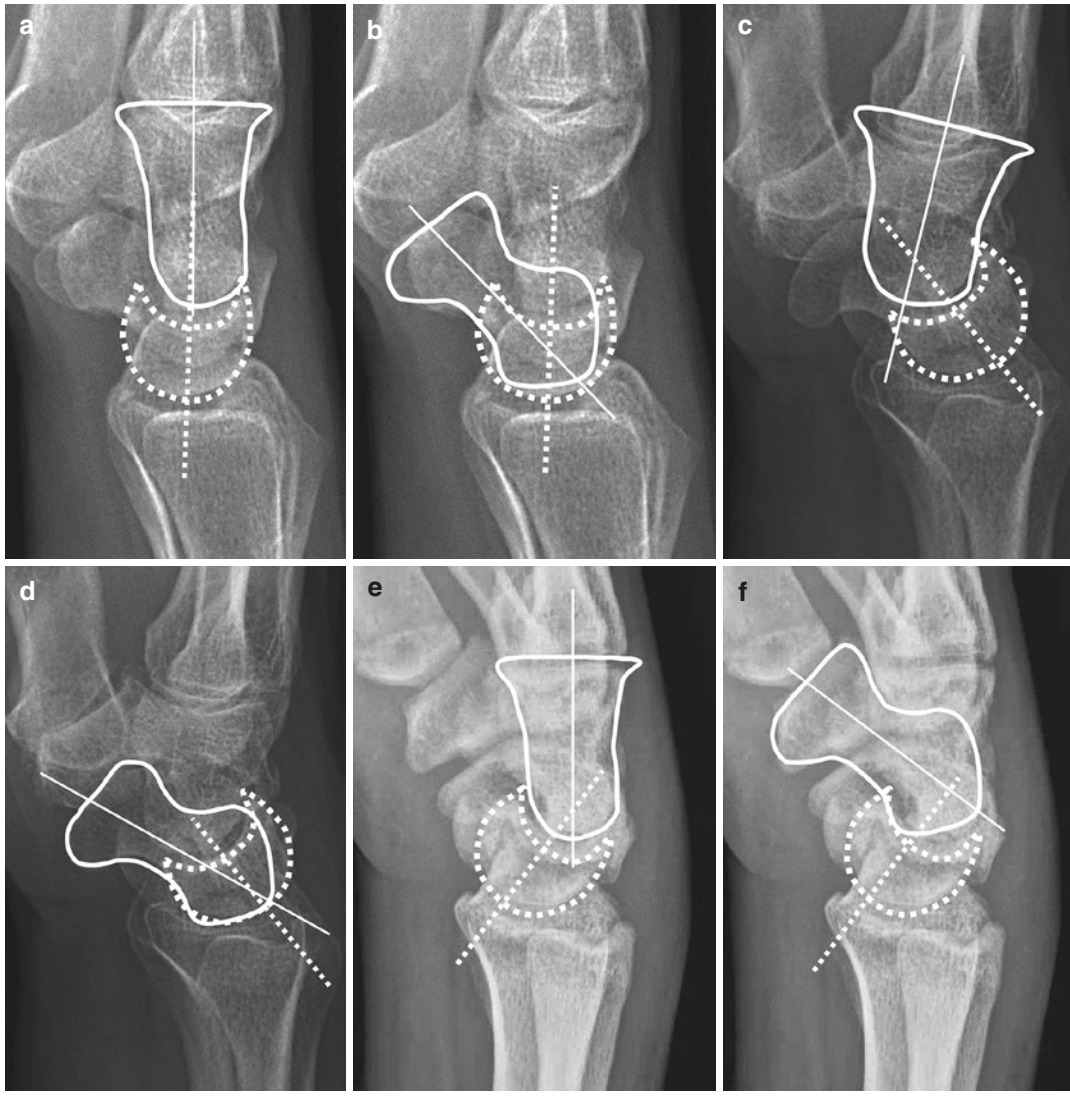


**Fig. 6.3** Normal lateral radiograph of the hand with capitolunate angle <30°(**a**) and scapholunate angle between 30 and 60°(**b**). Lateral radiograph with VISI shows capitolunate angle >30°(**c**) and scapholunate angle <30°(**d**). Lateral radiograph with DISI shows capitolunate angle >30°(**e**) and scapholunate angle >60°(**f**)

points of the radial articular surface and a line perpendicular to the midshaft of the radius. Normally this angle ranges from 11° of volar tilt to 4° of dorsal tilt [8] (Fig. 6.4d).

Ulnar variance is the difference in length between the distal radius and ulna. This variance is relevant to the force distribution across the wrist [10]. Ulnar variance is characterized by the differences in apparent lengths of the distal ulna and radius. Ulnar variance is defined as neutral, positive, or negative on the basis of whether the distal articular surface of the ulna is aligned with the distal articular surface of the radius on a neutral posteroanterior imaging (Fig. 6.4a–c) [11]. The ulna is shorter than the radius in negative ulnar variance and longer in positive ulnar variance. Positive variance is defined when the level of the ulna is >2.5 mm beyond the distal articular surface of the radius at the distal radioulnar joint (DRUJ). Negative variance is when the ulnar articular surface is >2.5 mm

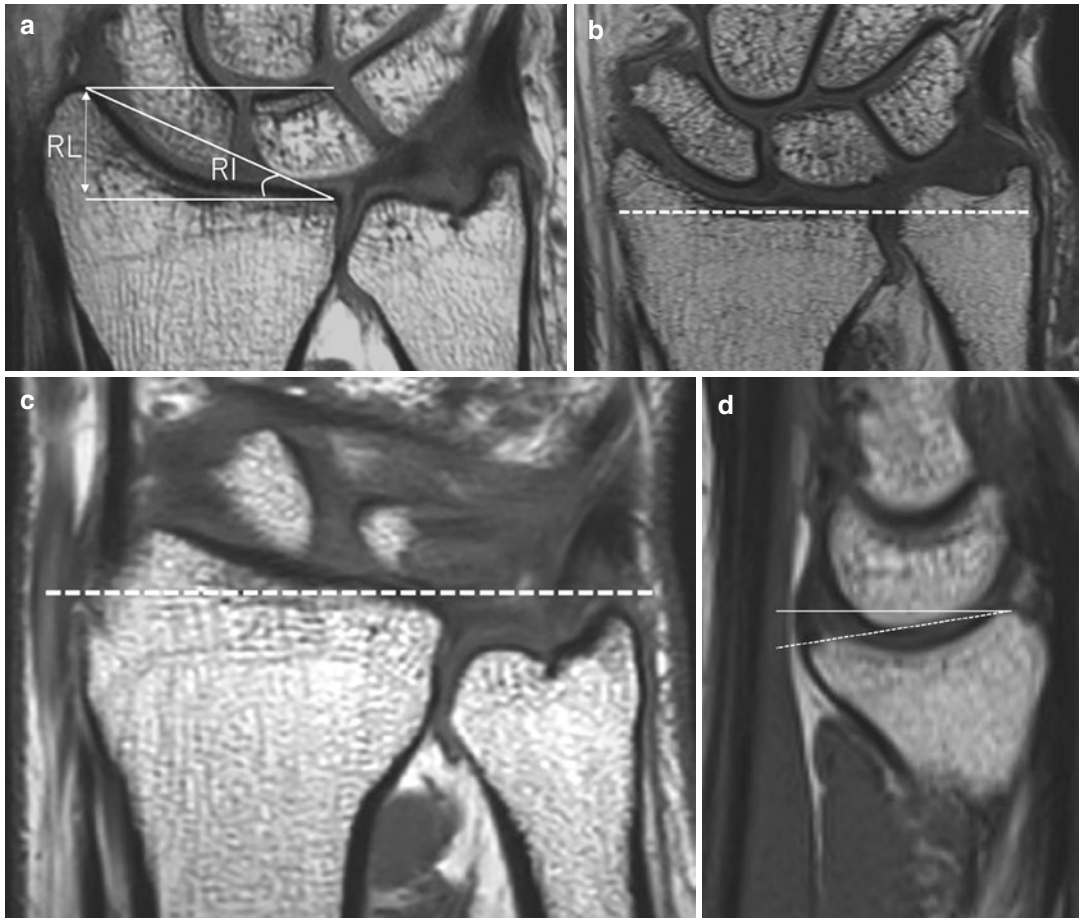


**Fig. 6.4** Measurements of the distal radius: RI radial inclination, RL radial length. Ulnar variance is neutral. (**a**) Ulnar variance on coronal T1-weighted images. Positive ulnar (**b**). Negative ulnar variance (**c**). Dotted lines: distal articular surface of the radius. Normal volar tilt on coronal T1-weighted image (**d**)

proximal to the distal articular surface of the radius at the DRUJ [12]. Normally, the radius and ulna are neutral (same length), or there is mild negative ulnar variance. Positive ulnar variance is known to play a key role in ulnar impaction syndrome [12, 13]. Negative ulnar variance has a historic association with Kienbock's disease, but this has been debated in recent orthopedic literature [14, 15].

The DRUJ is formed by the articulation of the sigmoid notch of the radius and ulnar head. This joint is stabilized by the soft tissue and ligamentous components of the triangular fibrocartilage complex (TFCC). It is intimately associated with the sixth extensor compartment, housing the extensor carpi ulnaris.

## Guyon's Canal

The ulnar nerve passes through a semirigid longitudinal tunnel known as Guyon's canal or the ulnar tunnel at the palmar aspect of the wrist. It is located superficial to the ulnar aspect of the carpal tunnel and extends from the palmar carpal ligament at the proximal edge of the pisiform to the origin of the hypothenar muscles at the level of the hamulus, approximately 4 cm in distance (Fig. 6.5) [16]. The ulnar nerve, artery, and, occasionally, communicating veins pass through Guyon's canal with accompanying fat tissue. The boundaries are formed by the palmar carpal ligament at the volar aspect, pisiform at the ulnar

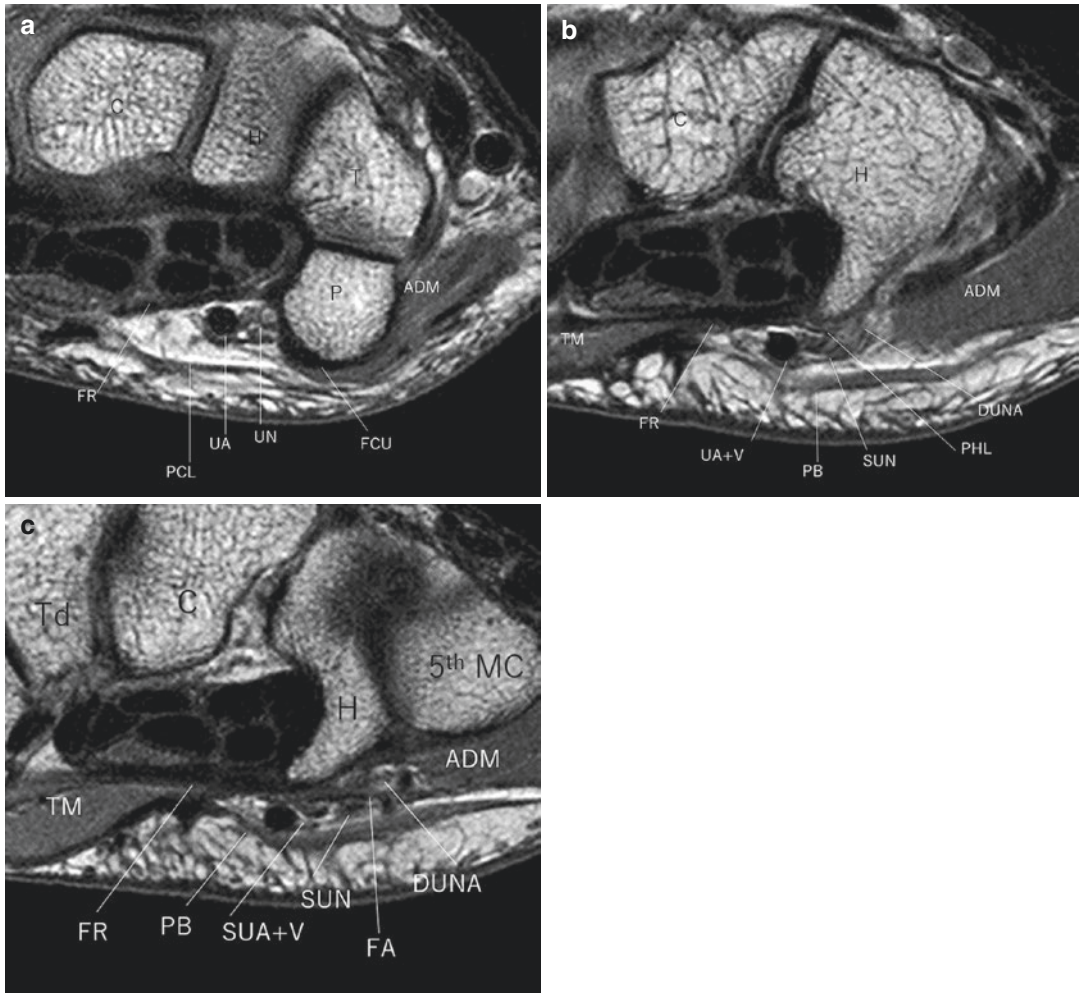


**Fig. 6.5** Normal anatomy of Guyon's canal. Axial proton density-weighted MR images of the wrist show anatomy of Guyon's canal in the proximal (**a**), middle-distal (**b**), and distal portion (**c**). Abbreviations: ADM Abductor digiti minimi muscle, DUNA Deep ulnar nerve and artery, FA Fibrous arch of flexor digiti minimi brevis muscle origin, FCU Flexor carpi ulnaris tendon, FR Flexor retinaculum or transverse carpal ligament, H Hamate, P Pisiform, C Capitate, T Triquetrum, Td Trapezoid, MC Metacarpal bone, PB Palmaris brevis muscle, PCL Palmar carpal ligament, SUA Superficial ulnar artery, SUN Superficial ulnar nerve, TM Thenar muscles, UA Ulnar artery, UN Ulnar nerve, V Vein

aspect, and flexor retinaculum of the carpal tunnel at the radial and deep aspect [10]. The ulnar nerve lies between the pisiform bone and the ulnar veins and artery. The transverse carpal ligament, or middle portion of the flexor retinaculum, forms the floor of Guyon's canal as well as the roof of the carpal tunnel; thus, the volumetric changes in one canal can affect the other [17, 18]. The flexor carpi ulnaris (FCU) tendon lies at the ulnar aspect of the ulnar nerve and artery in the forearm and inserts on the pisiform. It partially blends with the palmar carpal ligament and forms the volar boundary of Guyon's canal (Fig. 6.5a) [10].

In the mid-level of Guyon's canal, between the pisiform and hook of hamate, the shape may be triangular or oval (Fig. 6.5b). The boundaries are formed at the volar aspect by the palmar carpal ligament, at the deep aspect by the pisohamate ligament, at the ulnar aspect by the abductor

digiti minimi muscle, and at the radial aspect by the flexor retinaculum of the carpal tunnel [19]. Here, the ulnar nerve and artery bifurcate into deep and superficial branches.

At the distal portion of Guyon's canal, the boundaries are formed by the palmaris brevis muscle at the volar and radial aspect, the abductor digiti minimi muscle at the ulnar aspect, and the flexor retinaculum and the hook of hamate dorsally (Fig. 6.5c) [10]. The superficial and deep canals containing the ulnar neurovascular bundles are separated by the fibrous arch of the flexor digiti minimi brevis muscle origin. The deep canal contains the deep motor nerve and artery, whereas the superficial canal contains the superficial sensory nerve and artery [19]. Just distal to the outlet of Guyon's canal, the superficial ulnar artery and the sensory nerve pass volar to the hook of hamate without protective tissues and are vulnerable to mechanical stress or trauma [20].

## Carpal Tunnel

The carpal tunnel is a fibro-osseous tunnel on the palmar side of the wrist. It is bounded by the eight carpal bones and a tough fibrous roof called the transverse carpal ligament (TCL). The carpal tunnel contains eight digital flexor tendons (two for each of the second through fifth rays), flexor pollicis longus (FPL) the radial and ulnar bursae, with the median nerve (Fig. 6.6) [21]. Its dorsal and lateral borders are formed by the scaphoid, triquetrum, lunate, and pisiform proximally and the trapezium, trapezoid, capitate, and hamate distally. This osseous configuration forms a tunnel-like groove called the *sulcus carpi*. The flexor retinaculum forms its palmar boundary and extends from the tuberosities of the scaphoid and the trapezium to the pisiform and the hook of the hamate [22]. In general, the width of the carpal tunnel is narrowest at the level of the hamate hook, located 1 cm beyond the middle of the distal row of the carpal bones about 20 mm [21]. The mean width of the tunnel is 25 mm at its proximal end and 26 mm at its distal border [23]. Variations in the hook of the hamate (hypoplastic, aplastic, or bipartite) in addition to variations in the attachment of the TCL could result in changes in carpal tunnel volume (Fig. 6.7a, b).

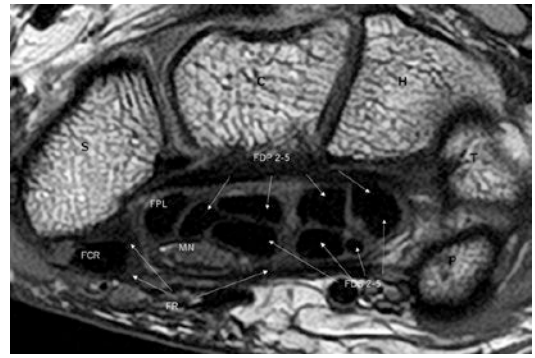


**Fig. 6.6** Normal anatomy of carpal tunnel on proton density-weighted axial image. Abbreviations: FCR Flexor carpi radialis, FDP Flexor digitorum profundus, FDS Flexor digitorum superficialis, FPL Flexor pollicis longus, FR Flexor retinaculum, MN Medial nerve, S Scaphoid, C Capitate, H Hamate, T Triquetrum, P Pisiform

The flexor retinaculum is differentiated in three segments: (1) a proximal thin segment called the palmar carpal ligament, (2) the middle tough segment called the TCL, and (3) the distal segment that consists of a thick aponeurosis between the thenar and hypothenar muscles, passing deep to the flexor carpi ulnaris and flexor carpi radialis. The TCL is a thick (2–4 mm) and strong fibrous band. It is attached to the pisiform bone and hook of the hamate medially. Laterally, it splits into two laminae, superficial and deep. The superficial lamina is attached to the tubercle of the scaphoid and trapezium. The deep lamina is attached to the groove on the trapezium. Those two laminae and the osseous groove form a tunnel for flexor carpi radialis (FRC) with its synovial sheath [21]. The volar aspect of the *sulcus carpi* is covered by the extrinsic ligaments, including the palmar lunotriquetral and palmar scaphotriquetral ligaments proximally and the capitate-scaphoid and capitate-trapezium ligaments distally. Usually, a small but variable amount of fatty tissue lies just volar to the capitate-trapezium ligament (Parona's fat pad).

The median nerve is the most volar structure in the carpal tunnel, located just deep to the flexor retinaculum and volar to the flexor digitorum superficialis (FDS) tendons. It is covered by a

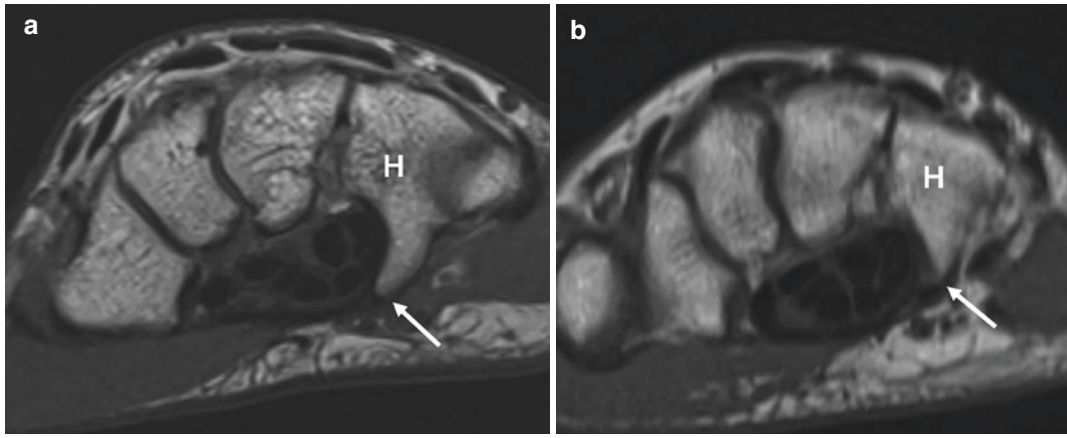


**Fig. 6.7** Normal (**a**) and hypoplastic (**b**) hook of hamate on axial T1-weighted images. Note the area of distal carpal tunnel is decreased in (**b**)

layer of cellulo-adipose tissue and adheres to the adjacent ulnar bursa [24]. It changes in position relative to the adjacent tendons on flexion or extension. In extension, the median nerve is usually located anterior to the index finger FDS tendon attached to the flexor retinaculum. In contradistinction, in the flexed position, the median nerve moves dorsally between the FDS of the second finger and flexor pollicis longus tendon. A palmar cutaneous branch arises from median nerve just proximal to the carpal tunnel. Distal to the carpal tunnel, the median nerve divides into medial and lateral branches. The medial branch terminates as two common palmar digital nerves supplying motor innervation to the second lumbrical and sensory innervation to the palm and fingers [25]. The lateral branch gives rise to the proper palmar digital nerves supplying motor innervation to the first lumbrical, sensory innervation to the lateral side of the hand and the thenar motor branch (TMB). The TMB, also referred to as the recurrent motor branch, supplies the abductor pollicis brevis and opponens pollicis muscles, the caput superficiale of the flexor pollicis brevis muscle, and the two radial lumbrical muscles.

Variations of the median nerve are common in the general population including the following four types: type 1 is a single TMB, type 2 has accessory branches of the median nerve at the distal carpal tunnel, type 3 has a high division of the median nerve, and type 4 has the median nerve and its accessory branches proximal to the carpal tunnel [26]. The prevalence of the type 3 variation, a high division of the median nerve resulting in a bifid median nerve, was reported to have a prevalence of 2.6% in a meta-analysis study [27]. In a study performed on 246 carpal tunnel release operations, five of seven patients with the bifid median nerve had an associated persistent median artery [28]. When the median artery persists, it is located on the ulnar aspect of the normal median nerve or between the bifid median nerve components, enveloped by a common perineurium [29]. The presence of hypertrophic muscle within the TCL was reported with a prevalence of 18.2% of hands, with higher prevalence of the TMB variants compared to those without it (23.4% vs 1.7%) [27]. Thus, it is important to recognize a bifid median nerve, persistent median artery, or hypertrophic muscle within the TCL with MRI or US preoperatively.

The four flexor digitorum profundus (FDP) and four FDS tendons arise from muscle bellies proximal to the carpal tunnel. They lie within the ulnar bursa, a sac-like structure lined with a synovial membrane, and are separated from the flexor pollicis longus tendon that resides within the radial bursa [22]. The ulnar bursa extends around the flexor tendons at the level of the carpal tunnel and is composed of three horizontally oriented invaginations of the synovial membrane: (1) a superficial

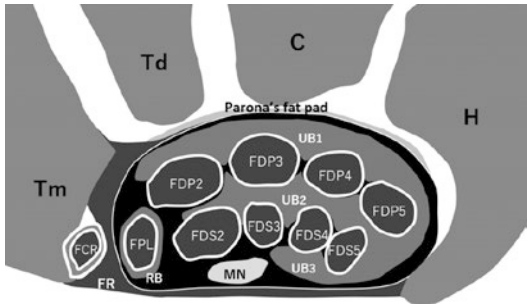


**Fig. 6.8** Schematic drawing of the carpal tunnel. Abbreviations: FCR Flexor carpi radialis, FDP Flexor digitorum profundus, FDS Flexor digitorum superficialis, FPL Flexor pollicis longus, FR Flexor retinaculum, MN Medial nerve, RB Radial bursa, UB Ulnar bursa, S Scaphoid, C Capitate, H Hamate, T Triquetrum, P Pisiform

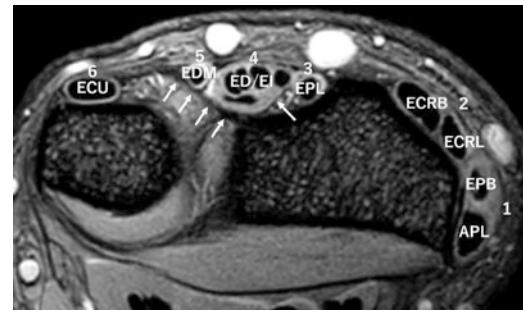


**Fig. 6.9** Extensor compartment anatomy. Axial T2*-weighted MR image through the level of the distal radioulnar joint showing the six extensor compartments. Arrows show the infratendinous flexor retinaculum. Note the fifth compartment for the extensor digiti minimi tendon (EDM) is purely fibrous

layer situated between the TCL of the flexor retinaculum and the FDS tendons, (2) a middle layer between the FDS tendons and the FDP tendons, and (3) a deep layer situated behind the FDP tendons (Fig. 6.8) [30]. Various patterns of communication between the radial and ulnar bursae, as well as between the bursae and individual tendon sheaths, have been reported. The connection between the ulnar and radial bursae and between the ulnar bursa and flexor digitorum tendon sheath of the fifth digit tendon is typical, with the lack of continuity of the second to fourth flexor tendon sheaths [31]. These communications are of clinical importance in explaining the spread of inflammation, infection, or neoplastic processes.

## Extensor Tendons and Extensor Retinaculum

The extensor tendons of the wrist are divided into six compartments along its dorsal aspect. These include the first compartment with the abductor pollicis longus (APL) and extensor pollicis brevis (EPB), the second compartment with the extensor carpi radialis longus (ECRL) and extensor carpi radialis brevis (ECRB), the third compartment with the extensor pollicis longus (EPL), the fourth compartment with the extensor digitorum and extensor indicis, the fifth compartment with the extensor digiti minimi, and the sixth compartment with the extensor carpi ulnaris (ECU). The extensor retinaculum (ER) is a thickening of the distal antebrachial fascia at the level of the inferior radioulnar joint that involves the extensor tendons over the radial, dorsal, and ulnar aspects of the wrist [32]. It consists of two layers, supratendinous and infratendinous (Fig. 6.9) (Table 6.1) [33].

On the radial side of the wrist, the ER attaches at the volar-radial border above the styloid process (Fig. 6.10(I)) blending with the antebrachial fascia, the palmar carpal ligament, and occasionally the fascia overlying the thenar compartment [32]. The ER lies over the tendons to insert into the dorsoradial bony protuberance on the distal radius (Fig. 6.10(II)). Superficial to the first extensor compartment, slips of the ER can form septa that extend between and separate the APL and EPB or even separate individual tendon slips of the APL. The prevalence of supranumerary tendon slips ranged from 74% to 77% for the APL and 2% to 27% for the EPB in cadavers [34–37]. Consistently higher prevalence of supernumerary tendon slips and septation has been reported in patients with De Quervain tenosynovitis. Chang et al. reported multiple tendon slips were also common on MRI, with a prevalence of 74–79% in a control group compared to 91% in a De Quervain tenosynovitis group [38]. In a previous study on CT, the osseous ridge at the floor of the first extensor compartment was found in 23.8% among the general population, with a statistically significant increase in females (19.8%

**Table 6.1** Extensor tendons

| |
|---|
| First compartment (1): Abductor pollicis longus (APL) and extensor pollicis brevis (EPB) tendon |
| Second compartment (2): Extensor carpi radialis longus and brevis tendons (ECRL, ECRB) |
| Third compartment (3): Extensor pollicis longus (EPL) tendon |
| Forth compartment (4): Extensor digitorum (ED) and extensor indicis (EI) tendon |
| Fifth compartment (5): Extensor digiti minimi (EDM) tendon |
| Sixth compartment (6): Extensor carpi ulnaris (ECU) tendon |

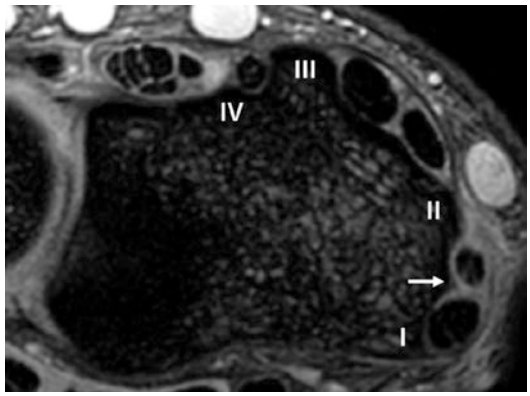


**Fig. 6.10** Attachment sites of the extensor retinaculum to the radius on T2*-weighted axial image. Note the osseous protuberance beneath the first extensor compartment (arrow). (I) The volar-radial border above the styloid process, (II) the dorsoradial bony protuberance on the distal radius, (III) Lister's tubercle of the radius, (IV) the osseous prominence on the radius, (I–II) the first compartment containing abductor pollicis longus tendon (APL) and extensor pollicis brevis tendon (EPB), (II–III) the second compartment containing extensor carpi radialis longus and brevis tendons (ECRL, ECRB), (III–IV) the third compartment containing extensor pollicis longus tendon (EPL)

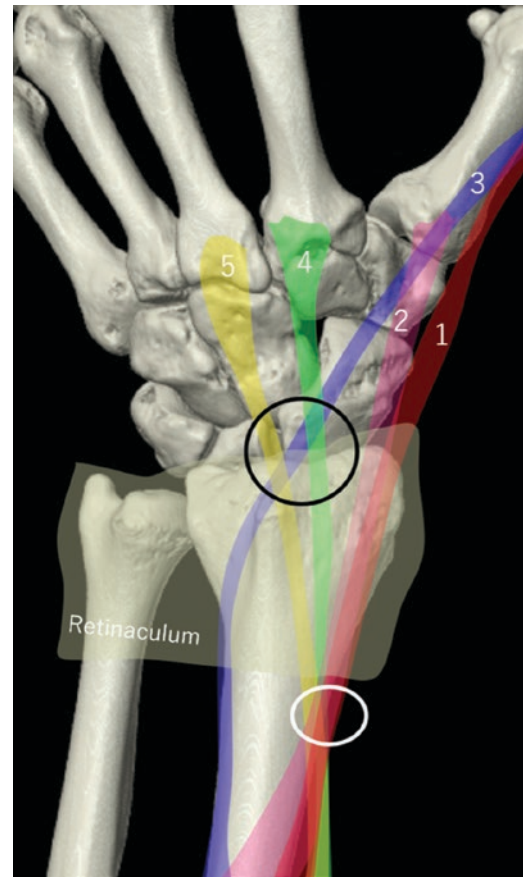


**Fig. 6.11** Anatomic diagram shows the distal (black circle) and proximal (white circle) intersections of the extensor tendons. (1) Red, abductor pollicis longus; (2) pink, extensor pollicis brevis; (3) blue, extensor pollicis longus; (4) green, extensor carpi radialis longus; (5) yellow, extensor carpi radialis brevis tendon

in males, 33.3% in females) [39]. An ultrasound anatomical study showed the association between the osseous ridge and the presence of the septation in the first extensor compartment; therefore, it can be an indirect sign of compartmentalization [40]. The bony ridge is observed also on MRI when the slice thickness is appropriate (Fig. 6.10).

The second extensor compartment is formed by the ER located between the dorsoradial bony protuberance (Fig. 6.10(II)) and Lister's tubercle of the radius (Fig. 6.10(III)). As previously noted, this compartment contains the ECRB and ECRL tendons. The insertion of the ER into Lister's tubercle is broad and extends along the entire expanse of the tubercle [32]. Lister's tubercle is an important osseous landmark to separate the second and third extensor compartments. The tendons of the first and second compartments cross each other 4–8 cm proximal to Lister's tubercle (Fig. 6.11) [41]. This intersection creates a vulnerability due to repetitive friction with supination and pronation, flexion, and extension [42]. Routine wrist MRI protocols may not extend proximally to offer full characterization of this region, emphasizing the importance of a detailed clinical history.

The ER crosses the EPL of the third extensor compartment with an attachment from Lister's tubercle (Fig. 6.10(III)) to the osseous prominence on the radius (Fig. 6.10(IV)) [43]. The EPL, ECRB, and ECRL tendons intersect distal to Lister's tubercle with communication of their tendon sheaths at the point of intersection (Fig. 6.11). Lister's tubercle acts as a pulley and therefore creates a vulnerability of the tendons in the setting of intersection syndrome [44].

The supratendinous portion of the ER crosses over the extensor digitorum and extensor indicis to form the fourth and fifth extensor compartments. The ER attaches to an osseous prominence at the dorsoulnar aspect of the radius [32]. The infratendinous portion of the ER is well described on images at the level of the fourth and fifth compartments. The supratendinous and infratendinous portions of the ER coalesce to separate the fourth and fifth extensor compartments [43]. The two portions of the retinaculum continue to surround the extensor digiti minimi tendon and form a purely fibrous fifth compartment.

The ECU tendon of the sixth extensor compartment lies within the subsheath along a groove at the dorsolateral aspect of the ulna. The two portions of the retinaculum meet to form the radial-sided attachment of this compartment [43]. The supratendinous portion of the ER extends over the ECU tendon blending fibers with the volar antebrachial fascia. Ulnarward, it inserts into the sheath of the flexor carpi ulnaris tendon, the pisiform, the pisometacarpal ligament, and the base of the fifth metacarpal [29]. The supratendinous and the infratendinous portions provide blending fibers with the subsheath of the ECU [32]. The ECU tendon centers in its groove in pronation and neutral position (Fig. 6.12) [45]. In supination, the tendon subluxes, and the extensor retinaculum is stretched. The "linea jugata" is the longitudinal fibrous

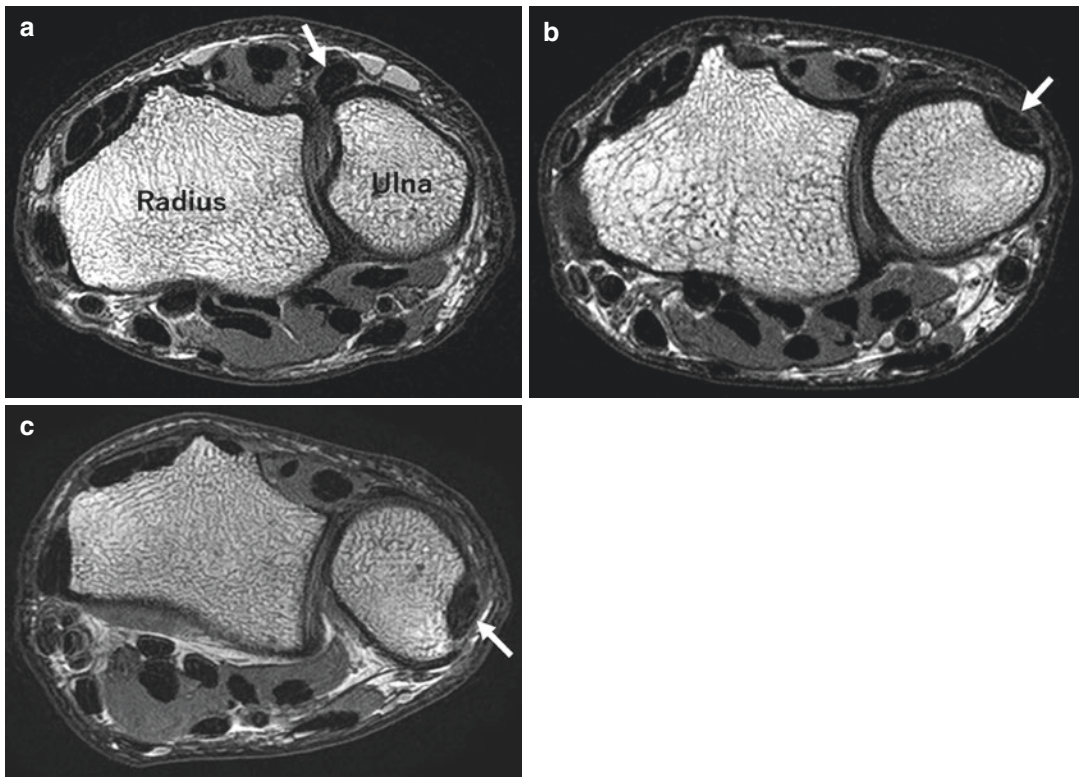


**Fig. 6.12** Location of the ECU tendon (arrow) with supination (**a**), neutral (**b**), and pronation (**c**)

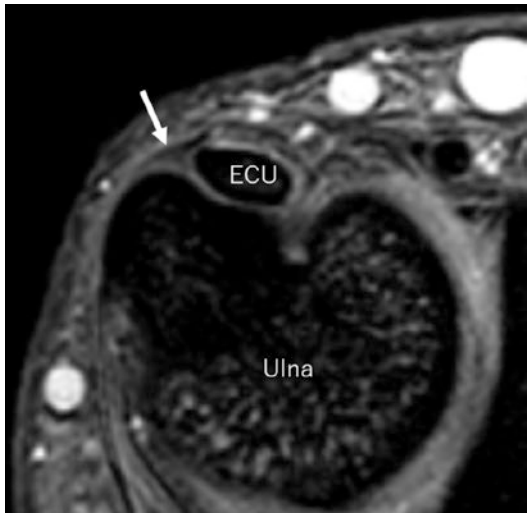


**Fig. 6.13** Linea jugata. T2*-weighted axial MR image shows the linea jugata (arrow) stabilizing the ulnar side of the ECU

structure that reinforces the ulnar insertion of the subsheath (Fig. 6.13) [46]. It is an important dynamic stabilizer that helps to prevent ECU tendon luxation during supination [33].

## Ligaments of the Wrist

Wrist ligaments are responsible for stability through complex motion about the radiocarpal, ulnocarpal, and DRUJ. The ligaments of the wrist have been classified into two types. Distinction has been made between the extrinsic (radiocarpal and ulnocarpal) and the intrinsic (intercarpal) ligaments (Table 6.2) (Figs. 6.14, 6.15, and 6.16).

## Intrinsic Ligaments

### Proximal Interosseous Ligaments

There are two proximal intrinsic interosseous wrist ligaments: the scapholunate (SL) ligament and the lunotriquetral (LT) ligament. The proximal intrinsic ligaments cover the dorsal, proximal, and volar aspects of their joints, respectively, leaving the distal aspect open to communicate with the midcarpal joint (Fig. 6.14a, b) [3].

The SL ligament is U-shaped on sagittal section and has three separate zones: dorsal, proximal, and volar components. The dorsal and volar zones are ligamentous, whereas the proximal zone is fibrocartilaginous [10]. The SL ligament is the primary stabilizer of the scapholunate joint. The dorsal zone is the thickest and strongest situated between the proximal pole of the scaphoid and the dorsal portion of the lunate [47]. The volar zone is thin and oriented obliquely from palmar to dorsal progressing from the scaphoid to the lunate; therefore, it is less easily observed on conventional MRI. It combines with the radioscapholunate ligament proximally and inserts on the scaphoid with small connections to the radioscaphocapitate ligament distally [48]. The proximal zone is fibrocartilaginous, similar to the TFCC histologically. DISI can occur due to alteration of SL ligament integrity, with flexion of the scaphoid and extension of the lunate and triquetrum. A recent cadaveric study showed scaphotrapeziotrapezoid ligament or distal intercarpal ligament resection, in association with SL ligament resection, produced DISI [49].

The LT ligament is V-shaped on sagittal section with three separate zones: dorsal, proximal, and volar. The dorsal and volar zones are ligamentous, and the proximal zone is fibrocartilaginous [50]. The volar region is the thickest part and transmits the extension movement of the triquetrum [51]. The dorsal component functions as a restraint to rotation. The dorsal and volar zones of the LT ligament are biomechanically more important than the proximal zone. The proximal zone shows a triangular morphology in >85% of subjects; however, a variety of shapes and MR appearances have been reported [52, 53]. LT ligament instability and the associated capsular damage, typically to the dorsal radiocarpal and dorsal intercarpal ligament, result in VISI. The proximal zone of both SL ligament and LT ligament is best demonstrated on coronal plane (Fig. 6.15b), and the dorsal and volar zones are best identified on axial plane (Fig. 6.16).

**Table 6.2** Intrinsic and extrinsic ligaments of the wrist. (Abbreviations in the figures)

| |
|---|
| Intrinsic ligaments |
| Proximal interosseous ligaments |
| Scapholunate ligament (SL) |
| Lunotriquetral ligament (LT) |
| Distal interosseous ligaments |
| Trapeziotrapezoid (TT) ligament |
| Trapezocapitate (TzC) ligament |
| Capitohamate (CH) ligament |
| Palmar midcarpal ligaments |
| Scaphotrapeziotrapezoid (STT) ligament |
| Scaphocapitate (SC) ligament |
| Triquetrocapitate (TC) ligament |
| Triquetrohamate (TH) ligament |
| Dorsal intercarpal/intrinsic ligaments (DIC) |
| Extrinsic ligaments |
| Radiocarpal |
| Dorsal radiocarpal (DRC) ligament |
| Radioscaphocapitate (RSC) ligament |
| Long radiolunate ligament (LRL) |
| Short radiolunate ligament (SRL) |
| Radial collateral ligament (RCL) |
| Radioscapholunate ligament |
| Ulnocarpal |
| Ulnocapitate (UC) ligament |
| Ulnolunate (UL) ligament |
| Ulnotriquetral (UT) ligament |

## Distal Interosseous Ligaments

There are three ligaments connecting the carpal bones of the distal row: trapeziotrapezoid (TT) ligament, trapezocapitate (TzC) ligament, and capitohamate (CH) ligament. Each ligament consists of at least a dorsal and a volar region. The dorsal and volar TT ligaments extend across the entire length of the dorsal and volar joint margin [3]. The TzC ligament includes three zones: the volar, dorsal, and the deep. The deep zone is the strongest crossing the central region of the joint in an angled notch. The CH ligament extends substantially onto the distal half of the volar and the dorsal cortices of the bone [54]. As with the TzC ligament, the deep CH ligament is a thick and square-shaped structure (Fig. 6.14b).

## Palmar Midcarpal Ligaments

The four palmar midcarpal ligaments course from the scaphoid or triquetrum to the distal carpal row: the scaphotrapeziotrapezoid (STT) ligament, the scaphocapitate (SC) ligament, the triquetrocapitate (TC) ligament, and the triquetrohamate (TH) ligament (Fig. 6.14a). There is no direct connection between the lunate and the distal carpal row [3]. The STT ligament attaches to the radial and ulnar cortices of the distal pole of the scaphoid proximally. It passes distally to the palmar and radial aspect of the trapezium and the palmar surface of the trapezoid [55, 56]. The SC ligament attaches to the distal pole of the scaphoid proximally and the palmar cortex of the body of the capitate distally. The TC ligament attaches proximally to the distal and radial corner of the triquetrum and the ulnar cortex of the capitate [57]. The triquetrohamate ligament attaches to the distal margin of the palmar cortex of the triquetrum and extends distally to attach to the palmar cortex of the hamate body [54].

## Dorsal Intercarpal/Intrinsic Ligaments

The dorsal intercarpal (DIC) ligaments attach the dorsal tubercle of the triquetrum proximally to the dorsal ridge and radial surface of the scaphoid and in half of individuals the dorsal cortex of the trapezoid (Figs. 6.14d and 6.15c) [3, 58]. The DIC ligaments play the role of a secondary stabilizer associated with the dorsal radiocarpal ligament; however, the SL ligament is the primary stabilizer of the scapholunate joint [48]. They form a lateral V-shaped structure with an apex in the triquetrum that stabilizes the dorsal scapholunate interval [58].

# Extrinsic Ligaments

## Radiocarpal Ligaments

On the volar side, the radioscaphocapitate (RSC) ligament and the long radiolunate (LRL) liga-


**Fig. 6.14** Schematic drawing of the intrinsic and extrinsic ligaments. Volar intrinsic ligaments (**a**), dorsal deep intrinsic ligaments (**b**), volar extrinsic ligaments (**c**), and dorsal intercarpal/intrinsic and extrinsic ligaments (**d**). Abbreviations: see Table 6.2 for ligaments

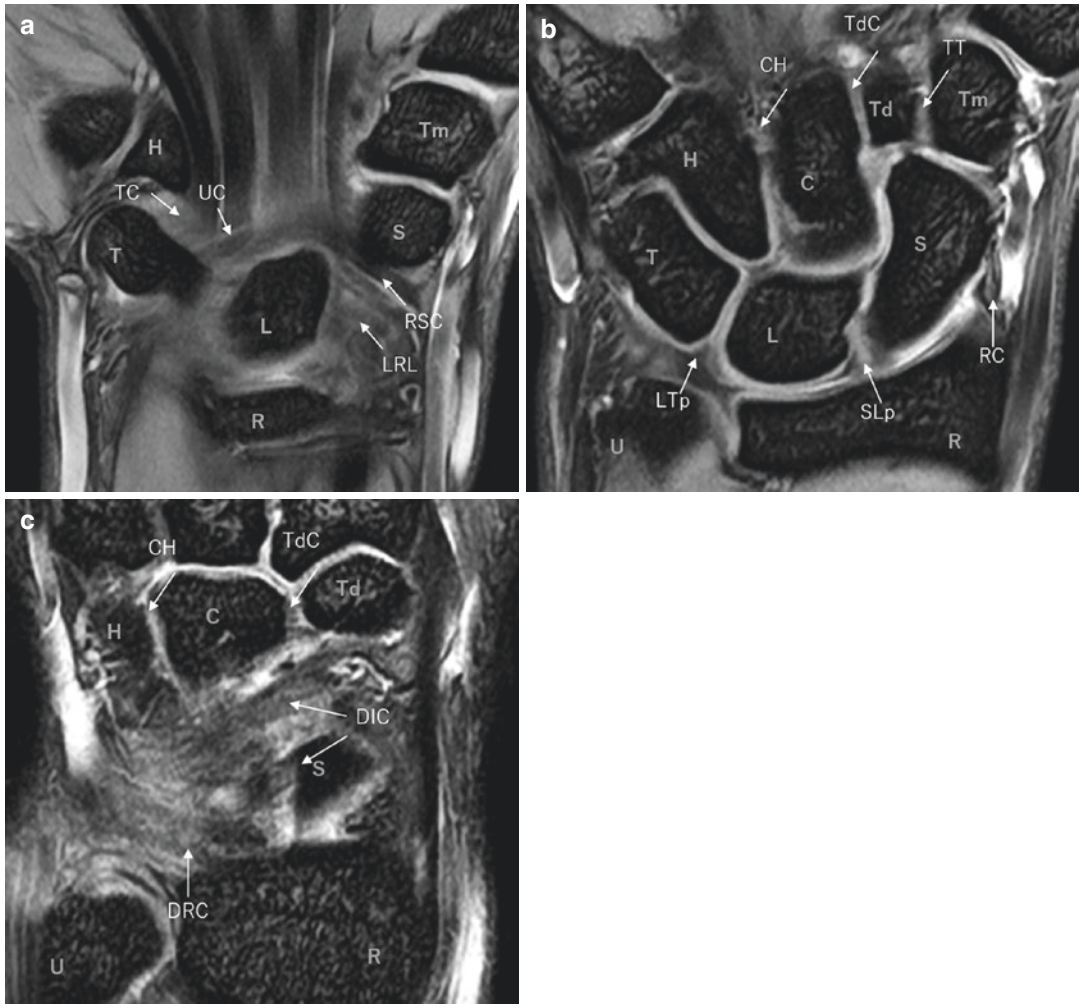


**Fig. 6.15** Anatomical images of the wrist ligaments on T2*-weighted coronal images. The proximal zone of both SL ligament and LT ligament are best demonstrated on this plane. Abbreviations: see Table 6.2 for ligaments. d dorsal zone, v volar zone, p proximal zone, R radius, L ulna, S scaphoid, L lunate, T triquetrum, Tm trapezium, Td trapezoid, C capitate, H hamate

ment are the two main ligamentous stabilizers of the scapholunate joint (Figs. 6.13c and 6.14a) [48]. The RSC ligament is the most radial extrinsic ligament and forms the entire radial radiocarpal and a part of the palmar radiocarpal joint capsule [55]. It extends diagonally from the radial styloid process to the region of the middle of the scaphoid fossa with connection to the fibers from the ulnocapitate (UC) ligament [57]. This structure is also referred to as the palmar arcuate ligament [59]. The LRL ligament, or volar radiolunotriquetral ligament, extends from the distal palmar rim of the radius to terminate in the lunate at the radial aspect of its palmar cortex over the lunate [60]. It plays a role in stabilization of the lunate in extension [49]. The short radiolunate (SRL) ligament originates proximally from the entire width of the lunate fossa of the distal radius and attaches to the radial half of the palmar cortex of the lunate [61]. The radial collateral ligament (RCL) extends from the tip of the styloid process of the radius and inserts on the distal pole and waist of the scaphoid and the palmar surface of the trapezium [62]. Another volar-

sided extrinsic ligament, the radioscapholunate ligament is found just ulnar to the long radiolunate ligament. There is some question as to whether this is a true ligament [63].

The dorsal radiocarpal (DRC) ligament (Figs. 6.14d and 6.15c), also called as the dorsal radiolunotriquetral ligament, is comprised of oblique fibers of approximately 1.5 mm thickness and attaches to the dorsal rim of the distal radius proximally and the dorsal cortex of the triquetrum, giving a firm attachment to the dorsoulnar corner of the lunate [64]. It is the most important dorsal extrinsic ligament to stabilize the lunate and scaphoid [65].

There are three identified ulnocarpal ligaments: the ulnocapitate (UC) ligament, the ulnolunate (UL) ligament, and the ulnotriquetral (UT) ligament (Figs. 6.14c and 6.15a). The UC ligament is the only ulnocarpal ligament that attaches directly to the ulnar head [66]. It attaches to the fovea region of the ulnar head proximally and interdigitates with the fibers of the RSC ligament distally as mentioned above.

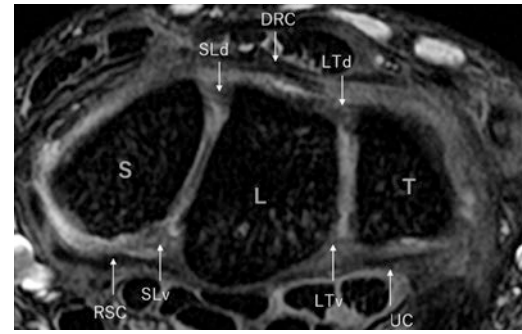


**Fig. 6.16** Anatomical image of the ligaments on T2*-weighted axial image at the level of the proximal carpal row. The dorsal and volar zones are best identified on this plane. Abbreviations: S Scaphoid, L Lunate, T Triquetrum, SL Scapholunate ligament, LT Lunotriquetral ligament, RSC Radioscaphocapitate ligament, DRC Dorsal radiocarpal ligament, UC Ulnocapitate ligament, d Dorsal zone, v Volar zone

## The Triangular Fibrocartilage Complex

The triangular fibrocartilage complex (TFCC) comprises the following structures: (1) triangular fibrocartilage disc, (2) radioulnar ligaments, (3) triangular ligament, (4) meniscal homologue, (5) ulnar collateral ligament (UCL), (6) volar ulnocarpal ligaments (ulnolunate and ulnotriquetral), and (7) extensor carpi ulnaris (ECU) tendon sheath (Figs. 6.17 and 6.18). The TFCC plays a role as the main stabilizer of the ulnar-sided wrist and the DRUJ. The TFCC articulates between the proximal carpal row and the distal ulna, facilitating smooth motion of the wrist, transmitting axial loads between the ulna and carpal bones, and serving as an extension of the proximal radial articular surface.

1. Triangular Fibrocartilage Disc

The triangular fibrocartilage disc appears as an asymmetric biconcave rectangular shape in the coronal plane (Fig. 6.17b, c). In contradistinction to the attachment of the dorsal and volar radioulnar ligaments mentioned later, there is a continuous transition from the central fibrocartilaginous disc to the hyaline cartilage of the sigmoid notch [67]. The shape of the disk remains constant throughout wrist motion when the ulnocarpal joint is stable. The morphology of the disc varies with ulnar variance [10]. The disc with the ulnar plus variance is thin and, therefore, more vulnerable to biomechanical stress.

2. Dorsal and Volar Radioulnar Ligaments

The dorsal and volar radioulnar ligaments form the main components of dorsal and volar marginal portion of the triangular fibrocartilage disc. The ligaments attach to the dorsal and volar rim of the distal radius directly at the level of the sigmoid notch and the middle and distal thirds of the styloid process via chondral-apophyseal entheses (Fig. 6.17a, b, d) [68]. The dorsal and volar radioulnar ligaments are well recognized in axial MR images (Fig. 6.18). The most superficial fibers of the dorsal radioulnar ligament contribute to the formation of the ECU tendon sheath ulnarly [22].

3. Triangular Ligament

The triangular ligament, a synonym of the ulnar side of the triangular fibrocartilage, anchors the

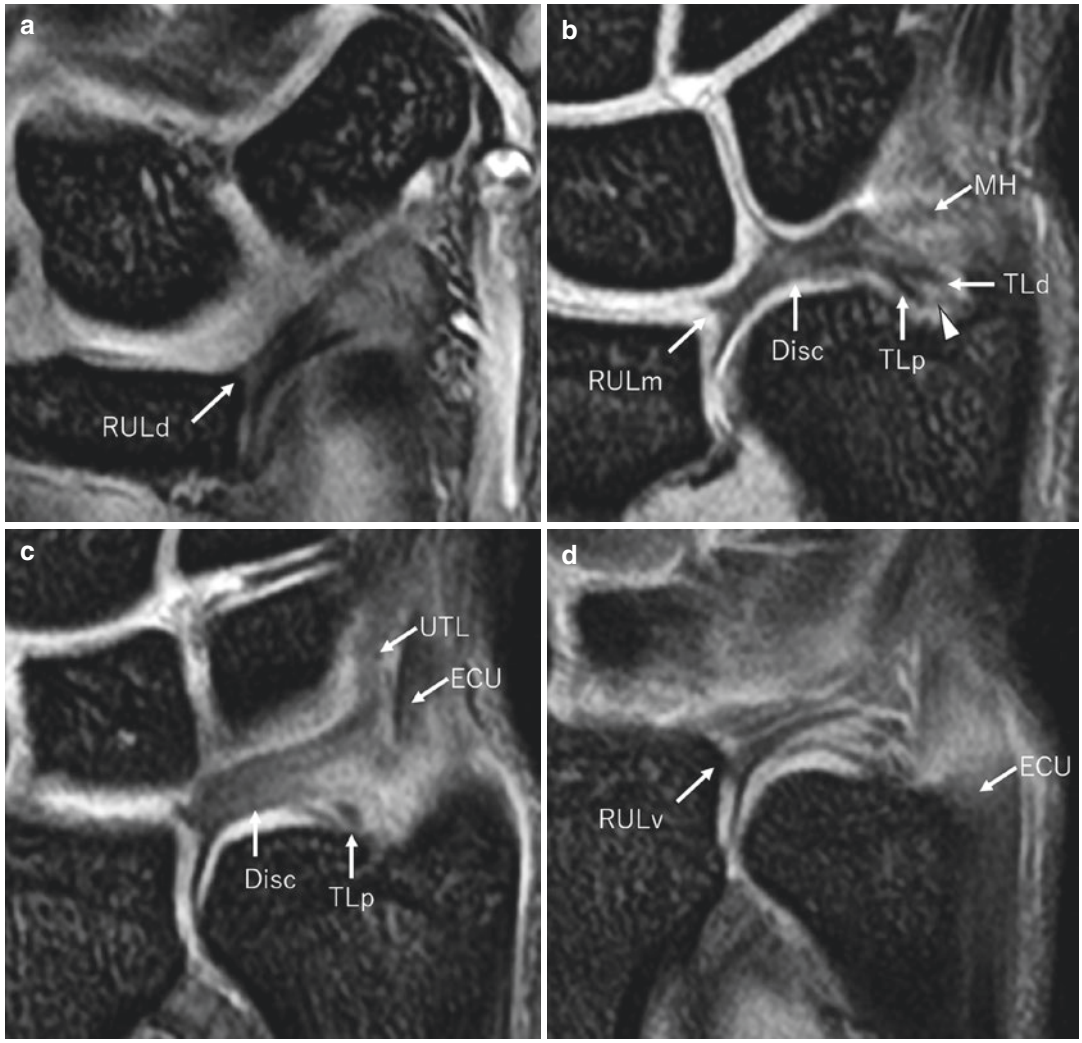


**Fig. 6.17** Coronal anatomical images of the TFCC. Abbreviations: RULd distal radioulnar ligament dorsal attachment, RULm distal radioulnar ligament middle attachment, RULv distal radioulnar ligament volar attachment, TLp triangular ligament proximal lamina, TLd triangular ligament distal lamina, MH meniscus homologue, UTL ulnotriquetral ligament, ECU extensor carpi ulnaris tendon

disc of triangular fibrocartilage to the ulnar styloid process. It extends along the entire surface to the most proximal aspect of the fovea of the styloid process and the tip [67]. The triangular ligament usually bifurcates into two laminae (proximal and distal) as the ligament extends toward the ulna (Fig. 6.17b, c) [69]. The distal lamina inserts into the fibro- or hyaline-like cartilage of the tip of the ulnar styloid [70]. The normal MRI appearance of the triangular ligament is a band with striated pattern (arrowhead). The internal signal is higher compared with the disc, due to its histological structure as a combination of collagen fibers and vascular-rich connective tissue [71].

4. Meniscal Homologue

The meniscal homologue is an inconsistent structure formed by a thickening of the ulnar side of the joint capsule. The meniscal homologue extends from the ulnar styloid to the dorsal edge of the triquetrum, the hamate, and the base of the fifth metacarpal [72]. It is best depicted in the coronal plane as a triangle-shaped structure with

hypointense signal (Fig. 6.17b). The prestyloid recess is a synovium-lined saccular space bordered by the meniscal homologue distally, the TFCC attachments to the ulnar styloid process proximally, and the central TFCC disk radially [73]. Commonly there is a direct connection to the rest of the radiocarpal compartment.

5. Ulnar Collateral Ligament

The concept of the UCL is nebulous but considered as the loose connective tissue that extends from the horizontal portion of the TFCC to join the subsheath of the ECU [74].

6. Volar Ulnocarpal Ligaments (ulnotriquetral and ulnolunate ligaments)

The UT and UL ligaments both originate proximally from the volar radioulnar ligament.

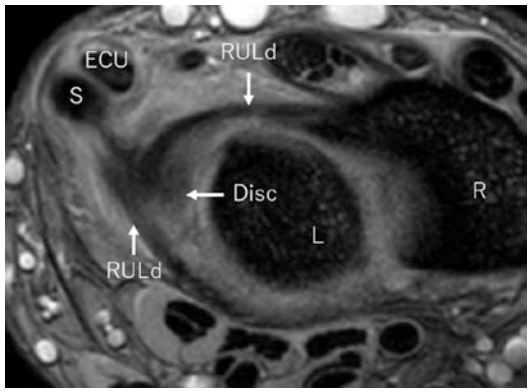


**Fig. 6.18** Axial image of the TFCC. Abbreviations: RULd distal radioulnar ligament dorsal attachment, RULv distal radioulnar ligament volar attachment, ECU extensor carpi ulnaris tendon, R radius, S styloid process

(3) They stabilize the lunate and, therefore, the proximal row of the carpal bones [61]. The UT ligament is intimately associated with the meniscal homologue. There is no direct attachment to the ulna. Assessment of their proximal attachment on MRI can be difficult because of the heterogeneous appearance due to the interspersed vascular loose connective tissue [75, 76]. Also, there is no clear demarcation between the UL and the UT ligaments proximally, but there are distinct attachment sites distally (Fig. 6.17c) [3].

7. Extensor Carpi Ulnaris (ECU) Subsheath

The ECU courses along the dorsolateral aspect of the ulnocarpal joint, is situated within the ulnar notch, and covered by fibrous tissue referred to as the ECU subsheath (Fig. 6.17c, d) [72]. As described above, a part of the dorsal radioulnar ligament and the dorsal radial metaphyseal arcuate ligament merge and reinforce the ECU subsheath [55]. They are further reinforced by the extensor retinaculum and ulnar collateral ligament which blends with the ECU subsheath. The ECU subsheath is an important stabilizer of the ulnar side of the TFCC.

## Imaging Protocols for the Wrist

Thin and contiguous slices with high signal-to-noise ratio are essential to evaluate the structures in the wrist joint as above discussed. Our routine noncontrast 3T wrist MR protocol is included in Table 6.3. Higher magnetic field such as 3T, with adequate coil selection such as wrist coil or microcoils for small field of view, is required. For

**Table 6.3** Routine wrist MR protocol

| Sequence | FOV | TR/TE | ST | SG | Matrix |
|---|---|---|---|---|---|
| Coronal T2FS | 10 cm | 3500–4000/60–90 | 3 mm | 0.3 mm | 320 |
| Coronal T1 | 10 cm | 450–500/13–15 | 3 mm | 0.3 mm | 320 |
| Coronal PD 3D | 10 cm | 2000–2500/18–30 | 1.4 mm | 0 | 288 |
| 3D reconstructed in axial and sagittal | | | | | |
| Sagittal T1 | 10 cm | 450–500/13–15 | 3 mm | 0.3 mm | 384 |
| Axial T2FS | 10 cm | 3500–4000/60–90 | 2.5 mm | 0.5 mm | 320 |
| Axial T1 | 10 cm | 600–850/10–15 | 2.5 mm | 0.5 mm | 384 |

Abbreviations: *FOV* field of view, *TR* repetition time, *TE* echo time, *ST* slice thickness, *SG* slice gap

the SLL injury evaluation, higher specificity at 3T compared with 1.5T is demonstrated in the recent meta-analysis study; however, that of MR arthrography with 3T was still superior. MRA may be considered when higher diagnostic performance is demanded to avoid invasive arthroscopy [77].

**Acknowledgments** All healthy wrist images were acquired on a Vantage Galan 3T, Canon Medical Systems.

Authors thank Ms. Christine Duxbury and Mr. Yurian Falls of Canon Medical for their supports in parameter optimizations and acquisitions.

## References

1. Metz VM, Wunderbaldinger P, Gilula LA. Update on imaging techniques of the wrist and hand. Clin Plast Surg. 1996;23(3):369–84.
2. Resnik CS. Wrist and hand injuries. Semin Musculoskelet Radiol. 2000;4(2):193–204.
3. Berger RA. The anatomy of the ligaments of the wrist and distal radioulnar joints. Clin Orthop Relat Res. 2001;383:32–40.
4. Viegas SF, Patterson RM, Hokanson JA, Davis J. Wrist anatomy: incidence, distribution, and correlation of anatomic variations, tears, and arthrosis. J Hand Surg Am. 1993;18(3):463–75.
5. Pfirrmann CW, Theumann NH, Chung CB, Trudell DJ, Resnick D. The hamatolunate facet: characterization and association with cartilage lesions--magnetic resonance arthrography and anatomic correlation in cadaveric wrists. Skeletal Radiol. 2002;31(8):451–6.
6. Goldfarb CA, Yin Y, Gilula LA, Fisher AJ, Boyer MI. Wrist fractures: what the clinician wants to know. Radiology. 2001;219(1):11–28.
7. Zanetti M, Hodler J, Gilula LA. Assessment of dorsal or ventral intercalated segmental instability configurations of the wrist: reliability of sagittal MR images. Radiology. 1998;206(2):339–45.
8. Weissman BNW, Sledge C. Orthopedic radiology. Philadelphia: Saunders; 1986. p. 111–67.
9. Solgaard S. Angle of inclination of the articular surface of the distal radius. Radiologe. 1984;24(7):346–8.
10. Vezeridis PS, Yoshioka H, Han R, Blazar P. Ulnar-sided wrist pain. Part I: anatomy and physical examination. Skeletal Radiol. 2010;39(8):733–45.
11. Mann FA, Wilson AJ, Gilula LA. Radiographic evaluation of the wrist: what does the hand surgeon want to know? Radiology. 1992;184(1):15–24.
12. Cerezal L, del Pinal F, Abascal F, Garcia-Valtuille R, Pereda T, Canga A. Imaging findings in ulnar-sided wrist impaction syndromes. Radiographics. 2002;22(1):105–21.
13. Imaeda T, Nakamura R, Shionoya K, Makino N. Ulnar impaction syndrome: MR imaging findings. Radiology. 1996;201(2):495–500.
14. van Leeuwen WF, Oflazoglu K, Menendez ME, Ring D. Negative ulnar variance and Kienböck disease. J Hand Surg Am. 2016;41(2):214–8.
15. Stahl S, Stahl AS, Meisner C, Hentschel PJH, Valina S, Luz O, Schaller HE, Lotter O. Critical analysis of causality between negative ulnar variance and Kienböck disease. Plast Reconstr Surg. 2013;132(4):899–909.
16. Gross MS, Gelberman RH. The anatomy of the distal ulnar tunnel. Clin Orthop Relat Res. 1985;196:238–47.
17. Brooks JJ, Schiller JR, Allen SD, Akelman E. Biomechanical and anatomical consequences of carpal tunnel release. Clin Biomech (Bristol, Avon). 2003;18(8):685–93.
18. Goitz RJ, Fowler JR, Li ZM. The transverse carpal ligament: anatomy and clinical implications. J Wrist Surg. 2014;3(4):233–4.
19. Zeiss J, Jakab E, Khimji T, Imbriglia J. The ulnar tunnel at the wrist (Guyon's canal): normal MR anatomy and variants. AJR Am J Roentgenol. 1992;158(5):1081–5.
20. Blum AG, Zabel JP, Kohlmann R, Batch T, Barbara K, Zhu X, et al. Pathologic conditions of the hypothenar eminence: evaluation with multidetector CT and MR imaging. Radiographics. 2006;26(4):1021–44.
21. Ghasemi-Rad M, Nosair E, Vegh A, Mohammadi A, Akkad A, Lesha E, et al. A handy review of carpal tunnel syndrome: from anatomy to diagnosis and treatment. World J Radiol. 2014;6(6):284–300.
22. Lewis OJ, Hamshere RJ, Bucknill TM. The anatomy of the wrist joint. J Anat. 1970;106(Pt 3):539–52.
23. Cobb TK, Dalley BK, Posteraro RH, Lewis RC. Anatomy of the flexor retinaculum. J Hand Surg Am. 1993;18(1):91–9.
24. Robbins H. Anatomical study of the median nerve in the carpal tunnel and etiologies of the carpal-tunnel syndrome. J Bone Joint Surg Am. 1963;45:953–66.
25. Demircay E, Civelek E, Cansever T, Kabatas S, Yilmaz C. Anatomic variations of the median nerve in the carpal tunnel: a brief review of the literature. Turk Neurosurg. 2011;21(3):388–96.
26. Lanz U. Anatomical variations of the median nerve in the carpal tunnel. J Hand Surg Am. 1977;2(1):44–53.
27. Henry BM, Zwinczewska H, Roy J, Vikse J, Ramakrishnan PK, Walocha JA, et al. The prevalence of anatomical variations of the median nerve in the carpal tunnel: a systematic review and meta-analysis. PLoS One. 2015;10(8):e0136477.
28. Beris AE, Lykissas MG, Kontogeorgakos VA, Vekris MD, Korompilias AV. Anatomic variations of the median nerve in carpal tunnel release. Clin Anat. 2008;21(6):514–8.
29. Gassner EM, Schocke M, Peer S, Schwabegger A, Jaschke W, Bodner G. Persistent median artery in the carpal tunnel: color Doppler ultrasonographic findings. J Ultrasound Med. 2002;21(4):455–61.

30. Resnick D. Roentgenographic anatomy of the tendon sheaths of the hand and wrist: tenography. Am J Roentgenol Radium Ther Nucl Med. 1975;124(1):44–51.
31. Aguiar RO, Gasparetto EL, Escuissato DL, Marchiori E, Trudell DJ, Haghighi P, et al. Radial and ulnar bursae of the wrist: cadaveric investigation of regional anatomy with ultrasonographic-guided tenography and MR imaging. Skeletal Radiol. 2006;35(11):828–32.
32. Palmer AK, Skahen JR, Werner FW, Glisson RR. The extensor retinaculum of the wrist: an anatomical and biomechanical study. J Hand Surg Br. 1985;10(1):11–6.
33. Taleisnik J, Gelberman RH, Miller BW, Szabo RM. The extensor retinaculum of the wrist. J Hand Surg Am. 1984;9(4):495–501.
34. Motoura H, Shiozaki K, Kawasaki K. Anatomical variations in the tendon sheath of the first compartment. Anat Sci Int. 2010;85(3):145–51.
35. Roy AJ, Roy AN, De C, Banerji D, Das S, Chatterjee B, et al. A cadaveric study of the first dorsal compartment of the wrist and its content tendons: anatomical variations in the Indian population. J Hand Microsurg. 2012;4(2):55–9.
36. Leao L. De Quervain's disease; a clinical and anatomical study. J Bone Joint Surg Am. 1958;40-A(5):1063–70.
37. Choi SJ, Ahn JH, Lee YJ, Ryu DS, Lee JH, Jung SM, et al. de Quervain disease: US identification of anatomic variations in the first extensor compartment with an emphasis on subcompartmentalization. Radiology. 2011;260(2):480–6.
38. Chang CY, Kheterpal AB, Vicentini JRT, Huang AJ. Variations of anatomy on MRI of the first extensor compartment of the wrist and association with DeQuervain tenosynovitis. Skeletal Radiol. 2017;46(8):1047–56.
39. Gurses IA, Turkay R, Inci E, Ors S, Onal Y, Ozel S, et al. Sex differences in the radial grooves in the first extensor compartment. Skeletal Radiol. 2016;45(7):955–8.
40. Rousset P, Vuillemin-Bodaghi V, Laredo JD, Parlier-Cuau C. Anatomic variations in the first extensor compartment of the wrist: accuracy of US. Radiology. 2010;257(2):427–33.
41. de Lima JE, Kim HJ, Albertotti F, Resnick D. Intersection syndrome: MR imaging with anatomic comparison of the distal forearm. Skeletal Radiol. 2004;33(11):627–31.
42. Lee RP, Hatem SF, Recht MP. Extended MRI findings of intersection syndrome. Skeletal Radiol. 2009;38(2):157–63.
43. Massaki AN, Tan J, Huang BK, Chang EY, Trudell DJ, Resnick DL. Extensor retinaculum of the wrist: gross anatomical correlation with MR imaging after ultrasound-guided tenography with emphasis on anatomical features in wrist dorsiflexion responsible for tendon impingement. Skeletal Radiol. 2013;42(12):1727–37.
44. Parellada AJ, Gopez AG, Morrison WB, Sweet S, Leinberry CF, Reiter SB, et al. Distal intersection tenosynovitis of the wrist: a lesser-known extensor tendinopathy with characteristic MR imaging features. Skeletal Radiol. 2007;36(3):203–8.
45. Pfirrmann CW, Theumann NH, Chung CB, Botte MJ, Trudell DJ, Resnick D. What happens to the triangular fibrocartilage complex during pronation and supination of the forearm? Analysis of its morphology and diagnostic assessment with MR arthrography. Skeletal Radiol. 2001;30(12):677–85.
46. Carneiro RS, Fontana R, Mazzer N. Ulnar wrist pain in athletes caused by erosion of the floor of the sixth dorsal compartment: a case series. Am J Sports Med. 2005;33(12):1910–3.
47. Berger RA. The gross and histologic anatomy of the scapholunate interosseous ligament. J Hand Surg Am. 1996;21(2):170–8.
48. Rajan PV, Day CS. Scapholunate interosseous ligament anatomy and biomechanics. J Hand Surg Am. 2015;40(8):1692–702.
49. Perez AJ, Jethanandani RG, Vutescu ES, Meyers KN, Lee SK, Wolfe SW. Role of ligament stabilizers of the proximal carpal row in preventing dorsal intercalated segment instability: a cadaveric study. J Bone Joint Surg Am. 2019;101(15):1388–96.
50. Johnstone DJ, Thorogood S, Smith WH, Scott TD. A comparison of magnetic resonance imaging and arthroscopy in the investigation of chronic wrist pain. J Hand Surg Br. 1997;22(6):714–8.
51. Zlatkin MB, Chao PC, Osterman AL, Schnall MD, Dalinka MK, Kressel HY. Chronic wrist pain: evaluation with high-resolution MR imaging. Radiology. 1989;173(3):723–9.
52. Smith DK, Snearly WN. Lunotriquetral interosseous ligament of the wrist: MR appearances in asymptomatic volunteers and arthrographically normal wrists. Radiology. 1994;191(1):199–202.
53. Yoshioka H, Tanaka T, Ueno T, Shindo M, Carrino JA, Lang P, et al. High-resolution MR imaging of the proximal zone of the lunotriquetral ligament with a microscopy coil. Skeletal Radiol. 2006;35(5):288–94.
54. Ritt MJ, Bishop AT, Berger RA, Linscheid RL, Berglund LJ, An KN. Lunotriquetral ligament properties: a comparison of three anatomic subregions. J Hand Surg Am. 1998;23(3):425–31.
55. Berger RA. The ligaments of the wrist. A current overview of anatomy with considerations of their potential functions. Hand Clin. 1997;13(1):63–82.
56. Drewniany JJ, Palmer AK, Flatt AE. The scaphotrapezial ligament complex: an anatomic and biomechanical study. J Hand Surg Am. 1985;10(4):492–8.
57. Taleisnik J. The ligaments of the wrist. J Hand Surg Am. 1976;1(2):110–8.
58. Viegas SF, Yamaguchi S, Boyd NL, Patterson RM. The dorsal ligaments of the wrist: anatomy, mechanical properties, and function. J Hand Surg Am. 1999;24(3):456–68.

59. Chang W, Peduto AJ, Aguiar RO, Trudell DJ, Resnick DL. Arcuate ligament of the wrist: normal MR appearance and its relationship to palmar midcarpal instability: a cadaveric study. Skeletal Radiol. 2007;36(7):641–5.
60. Mak WH, Szabo RM, Myo GK. Assessment of volar radiocarpal ligaments: MR arthrographic and arthroscopic correlation. AJR Am J Roentgenol. 2012;198(2):423–7.
61. Shahabpour M, De Maeseneer M, Pouders C, Van Overstraeten L, Ceuterick P, Fierens Y, et al. MR imaging of normal extrinsic wrist ligaments using thin slices with clinical and surgical correlation. Eur J Radiol. 2011;77(2):196–201.
62. Siegel DB, Gelberman RH. Radial styloidectomy: an anatomical study with special reference to radiocarpal intracapsular ligamentous morphology. J Hand Surg Am. 1991;16(1):40–4.
63. Berger RA. Arthroscopic anatomy of the wrist and distal radioulnar joint. Hand Clin. 1999;15(3):393–413, vii.
64. Mizuseki T, Ikuta Y. The dorsal carpal ligaments: their anatomy and function. J Hand Surg Br. 1989;14(1):91–8.
65. Mitsuyasu H, Patterson RM, Shah MA, Buford WL, Iwamoto Y, Viegas SF. The role of the dorsal intercarpal ligament in dynamic and static scapholunate instability. J Hand Surg Am. 2004;29(2):279–88.
66. Garcia-Elias M. Soft-tissue anatomy and relationships about the distal ulna. Hand Clin. 1998;14(2):165–76.
67. Benjamin M, Evans EJ, Pemberton DJ. Histological studies on the triangular fibrocartilage complex of the wrist. J Anat. 1990;172:59–67.
68. Horiuchi S, Nimura A, Tsutsumi M, Suzuki S, Fujita K, Nozaki T, et al. Anatomical relationship between the morphology of the styloid process of the ulna and the attachment of the radioulnar ligaments. J Anat. 2020;237:1032–9.
69. Yoshioka H, Tanaka T, Ueno T, Carrino JA, Winalski CS, Aliabadi P, et al. Study of ulnar variance with high-resolution MRI: correlation with triangular fibrocartilage complex and cartilage of ulnar side of wrist. J Magn Reson Imaging. 2007;26(3):714–9.
70. Nakamura T, Takayama S, Horiuchi Y, Yabe Y. Origins and insertions of the triangular fibrocartilage complex: a histological study. J Hand Surg Br. 2001;26(5):446–54.
71. Cody ME, Nakamura DT, Small KM, Yoshioka H. MR imaging of the triangular fibrocartilage complex. Magn Reson Imaging Clin N Am. 2015;23(3):393–403.
72. Zhan HL, Li WT, Bai RJ, Wang NL, Qian ZH, Ye W, et al. High-resolution 3T magnetic resonance imaging of the triangular fibrocartilage complex in Chinese wrists: correlation with cross-sectional anatomy. Chin Med J (Engl). 2017;130(7):817–22.
73. Milz S, Sicking B, Sprecher CM, Putz R, Benjamin M. An immunohistochemical study of the triangular fibrocartilage complex of the wrist: regional variations in cartilage phenotype. J Anat. 2007;211(1):1–7.
74. Daunt N. Magnetic resonance imaging of the wrist: anatomy and pathology of interosseous ligaments and the triangular fibrocartilage complex. Curr Probl Diagn Radiol. 2002;31(4):158–76.
75. Chidgey LK, Dell PC, Bittar ES, Spanier SS. Histologic anatomy of the triangular fibrocartilage. J Hand Surg Am. 1991;16(6):1084–100.
76. Kauer JM. The articular disc of the hand. Acta Anat (Basel). 1975;93(4):590–605.
77. Hafezi-Nejad N, Carrino JA, Eng J, Blackmore C, Shores J, Lifchez SD, et al. Scapholunate interosseous ligament tears: diagnostic performance of 1.5 T, 3 T MRI, and MR arthrography-A systematic review and meta-analysis. Acad Radiol. 2016;23(9):1091–103.